Nanoscale

RSC Publishing

COMMUNICATION

View Article Online
View Journal

Semiconducting quantum confined silicon–tin alloyed nanocrystals prepared by ns pulsed laser ablation in water

Cite this: DOI: 10.1039/c3nr00891f

Received 20th February 2013
Accepted 27th May 2013

DOI: 10.1039/c3nr00891f

www.rsc.org/nanoscale

V. Švrček,*[a] D. Mariotti,[b] R. A. Blackley,[c] W. Z. Zhou,[c] T. Nagai,[a] K. Matsubara[a] and M. Kondo[a]

Here we demonstrate the material's synthetic feasibility for semiconducting alloyed silicon–tin nanocrystals (SiSn-NCs) with quantum confinement effects. An environmentally friendly synthesis is achieved by ns laser ablation of amorphous SiSn in water at ambient conditions. Plasmas generated in the liquid by laser pulses are characterized by spatial confinement with very high pressure (GPa), which allowed the growth of the SiSn-NCs *via* kinetic pathways. We further illustrate that surface engineering by a direct-current atmospheric pressure microplasma is capable of tailoring the SiSn-NCs surface properties without the need for lengthy surfactants, resulting in room temperature photoluminescence (PL); the PL peak wavelength is red-shifted by more than 250 nm with respect to the PL peak wavelengths observed for comparable elemental silicon nanocrystals.

Introduction

Silicon-based technologies have reached a very well-established and mature status, and currently dominate the semiconductors market. While bulk silicon-based optoelectronic structures are fundamentally disadvantaged from a materials point of view, there is a strong interest in producing novel optoelectronic structures that could be easily integrated within the existing silicon technology. This would benefit from the existing know-how and well-advanced industrial infrastructure. Bulk silicon's indirect bandgap is the main limitation to silicon light emission–absorption properties and a range of different approaches have been proposed to overcome this weakness. Notably, the use of either bulk alloying or quantum confinement (separately) has been extensively studied to manipulate the character of the silicon energy bandgap.[1–3] Specifically, alloying bulk Si with another material offers an opportunity for decreasing the bandgap, while nanostructuring to sizes below the quantum confinement limit (~10 nm) offers the possibility to open up the energy bandgap. Furthermore, both alloying and nanostructuring challenge the nature of silicon's indirect energy band gap.[4] Consequently the possibility of the combined effects due to Si-alloying and quantum confinement might result in highly desirable opportunities to precisely tune the energy levels and optoelectronic properties.[5] Furthermore, future silicon-based nanotechnology requires materials with precisely engineered bandgaps below that of silicon (1.1 eV). Since the concentration of Sn can be used to narrow the Si bandgap, so-called composition bandgap tuning, the $Si_{1-x}Sn_x$ alloy system would be an interesting candidate to meet these desired requirements while maintaining a good degree of compatibility with current silicon technologies.[2] Importantly, SiSn bulk alloys undergo a real transition from indirect to direct bandgap behaviour with enhanced opto-electronic conversion efficiency. However, due to the large difference in lattice constant between the Si and Sn, and the thermodynamic instability of the Si–Sn system at room temperature, $Si_{1-x}Sn_x$ alloys are inherently metastable. Early attempts to prepare $Si_{1-x}Sn_x$ *via* Si_2H_6 at a broad range of growth conditions invariably yielded amorphous and phase-segregated films. To date, only a few claims of bulk alloyed SiSn thin films have been published.[2,6] Recent research has demonstrated the successful development of GeSn and SiGeSn alloyed films, which show great potential in opto-electronic applications such as high-performance near-IR photodetectors.[7,8] Nevertheless, reports on the synthesis of nanoscale SiSn are extremely limited and only demonstrate the possibility of Sn-rich nanoparticles with metallic behaviour.[9] An alloyed and crystalline SiSn semiconductor phase is required to display relevant optoelectronic characteristics and to exhibit quantum confinement states as observed for semiconducting nanocrystals; Sn-rich nanocrystals or metallic-like nanocrystals are not expected to exhibit the required quantum characteristics and bandgap requirements in the context of optoelectronic applications previously introduced. Furthermore, alloyed nanocrystals with narrower energy bandgaps, compared to

[a]Research Center for Photovoltaic Technologies, AIST, Tsukuba, 305-8568, Japan. E-mail: vladimir.svrcek@aist.go.jp

[b]Nanotechnology & Integrated Bio-Engineering Centre-NIBEC, University of Ulster, UK

[c]EaStCHEM, School of Chemistry, University of St Andrews, St Andrews, Fife KY16 9ST, UK

corresponding elemental nanocrystals, would enhance the absorption of lower energy photons and could lead to the development of new types of solar cells with carrier multiplication (CM) effects.[10] Since CM requires strong quantum confinement (*e.g.* in the blue spectral region for elemental silicon nanocrystals), the use of alloys can shift the CM threshold to lower photon energies and therefore has the potential to improve significantly solar cell conversion efficiencies.[11] At the same time, water stability of luminescent colloidal nanocrystals is a key factor for nanocrystals to succeed as fluorescent biological probes in either long-term or real-time cellular labelling.[12] It is clear that in order to meet the requirements of each potential application, the fabrication process is a major concern. It should be noted that the nucleation and growth conditions of nanoscale structures often depart from the formation requirements of the corresponding bulk materials. It follows that while thermal methods (*e.g.* chemical vapour deposition) have been very successful for thin-film growth, highly non-equilibrium approaches have often been applied for the synthesis of nanoparticles. For instance, laser ablation in liquid media is a technique that can prepare colloidal elemental silicon nanocrystals with strong quantum confinement effects in a single-step process,[13,14] and allows for the nanocrystals to be synthesized in a clean environment resulting in outstanding purity of the products.[15–18] For these reasons, laser ablation in liquid presents several desirable characteristics to achieve alloying of quantum confined nanocrystals.

Another crucial factor for nanocrystals in general is represented by surface effects, which can strongly overlap with quantum confinement effects and eventually with nanocrystal alloying effects.[19,20] The ratio of surface atoms to the total number of atoms in nanocrystals with size below the quantum confinement size (<10 nm) is very large, and surface effects can play a significant role in determining the optoelectronic properties. Our recent research has therefore focused on viable technologies for surface engineering of nanoparticles at quantum confinement size.[19,21] We have successfully demonstrated approaches that allow for 3-dimenstional (3D) surface engineering of silicon nanocrystals (Si-NCs) directly in liquid, which relys on a direct-current (DC) atmospheric-pressure microplasma coupled to the liquid media.[21,22] This technique shows the capability of effective surface chemistry by providing a uniform passivation layer without using any lengthy surfactants that could hinder or complicate carrier dissociation and transport, as required for a range of applications and in particular for photovoltaics (PVs).[19,21]

In this manuscript, silicon-based quantum confined binary systems with Sn and surface control without the use of surfactants have been assessed together in the attempt of improving nanoscale silicon opto-electronic properties. In particular we report on our investigation of quantum confined SiSn alloyed semiconducting nanocrystals (SiSn-NCs) prepared by pulsed ns laser ablation in water of amorphous SiSn targets. We demonstrate the surface engineering of the SiSn-NCs resulting in room temperature PL, which shows a red shift of more than 250 nm compared to elemental Si-NCs prepared under the same conditions. Our results represent one of the first efforts in the synthesis of free-standing (or colloidal) semiconducting alloyed SiSn nanocrystals with quantum confinement effects.

Experimental results and discussion

Fig. 1a shows a typical TEM image of the as-prepared SiSn-NCs after evaporation of the water. The SiSn-NCs are in most cases spherical with a relatively large size distribution. Namely, ns pulsed laser ablation in water results in nanoparticles with diameter ranging from 2 nm to 70 nm with a mean value of about 17 nm. It has to be noted that the larger particles are actually aggregates of smaller crystallites with sizes not exceeding 10 nm. Energy dispersive X-ray spectroscopy (EDS) of the synthesized SiSn-NCs indicates the presence of both Si and Sn (Fig. 1b). Since the initial concentration of Sn in the target is relatively small, the Sn peak in the EDS spectrum is expected to be weak as observed in Fig. 1b (Sn indicated by arrow). EDS analysis shows other peaks such as copper (Cu) potassium (Na) and calcium (Ca) which mostly originate from the TEM grid. It

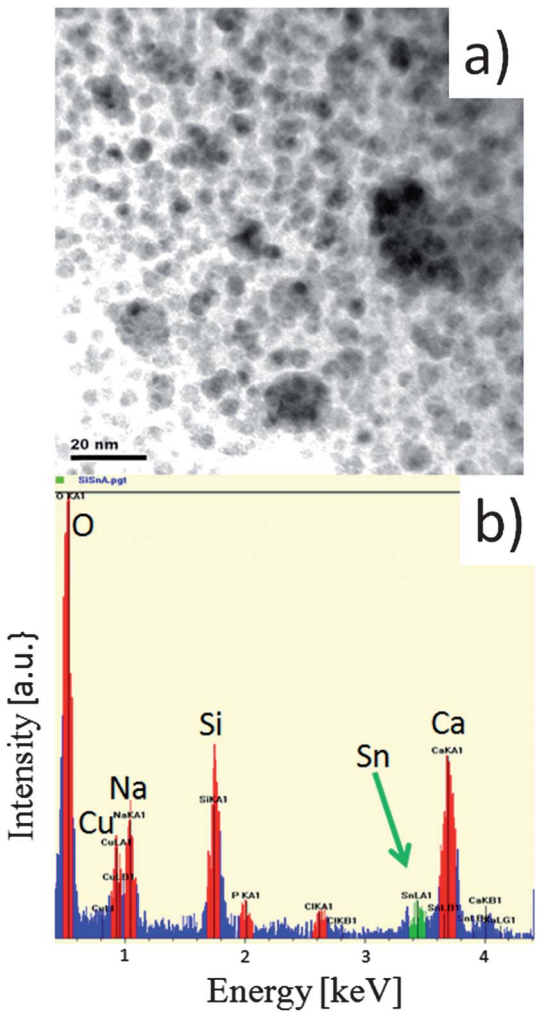

Fig. 1 (a) Transmission electron microscopy (TEM) image of SiSn nanocrystals produced by pulsed ns laser ablation in water of SiSn targets and dispersed on a TEM grid. (b) Corresponding energy-dispersive X-ray spectrum.

should be stressed that, as reported elsewhere, laser ablation in water represents a very clean approach for nanoparticle synthesis resulting in high purity nanocrystals[15,18] with very limited chances for contamination; therefore it is highly unlikely that the observed peaks (Cu, Na and Ca) originate from other Si-based alloys. Furthermore the elemental concentration of oxygen (O) is also observed which may indicate that the nanoparticles have undergone a degree of oxidation and the oxide may have formed after nanoparticle formation when exposed to water.

Raman spectroscopy provides a rapid and non-destructive measure of the synthesized SiSn-NCs and can provide indications of the nanocrystal size. Raman theoretical studies and experimental measurements were successfully applied for bulk SiSn layers.[2] Their studies showed a typical peak around 400 cm^{-1} for $Si_{0.7}Sn_{0.3}$.[2] This 400 cm^{-1} peak, generally attributed to alloyed SiSn,[2] was not observed in our measurement and only one Raman peak at 518 cm^{-1} was detected, which is located in the region where crystalline silicon and Si-NCs exhibit their Raman peaks. Fig. 2 shows the corresponding normalized Raman spectrum of the SiSn-NCs sample together with that of a crystalline Si wafer. A clear shift from the crystalline Si peak can be observed. The effect of SiSn alloying in the Raman spectra of nanocrystals may be difficult to interpret in this case. This is because SiSn alloying may be expected to produce a peak, depending on the relative concentration, between the typical Sn signal (400 cm^{-1}) and the Si signal (520 cm^{-1}); this would be consistent with our results in Fig. 2, whereby a small Sn concentration has produced a small downshift from 520 cm^{-1}. However, the Si-related Raman peak is also expected to asymmetrically broaden and downshift to a lower frequency (<520 cm^{-1}) for nanocrystals with sizes in the quantum confinement regime. It follows that Raman spectroscopy can only support either the formation of alloyed SiSn (not necessarily nanoparticles) or potentially the formation of elemental Si-NCs with quantum confinement. It is well known that the Raman-active mode in bulk Si occurs at the centre of the Brillouin zone ($q = 0$), leading to a sharp Raman scattering peak at 520 cm^{-1} (see Fig. 2). Crystal momentum is no longer conserved in Si-NCs and phonon modes become allowed away from the Brillouin zone centre ($q \neq q_0$), which leads to the downshift and widening of the Raman peak with decreasing nanocrystals size.[13,18] On the other hand, one should take into consideration that Raman theoretical models failed to capture the proper line shape of the low-frequency tail of the Raman peaks for very small Si nanocrystals (<3 nm). An in-depth Raman analysis and theoretical study of SiSn-NCs, which have yet to be reported, could face similar challenges and a correct evaluation of SiSn-NCs Raman modes may be as complicated as for elemental Si-NCs. Additionally Raman results are very sensitive to subtle differences in crystal structure, defects, composition, and local environmental conditions. Similar problems are expected for alloyed SiSn-NCs and in our case a downshift to 518 cm^{-1} and asymmetrical broadening was recorded (Fig. 2).

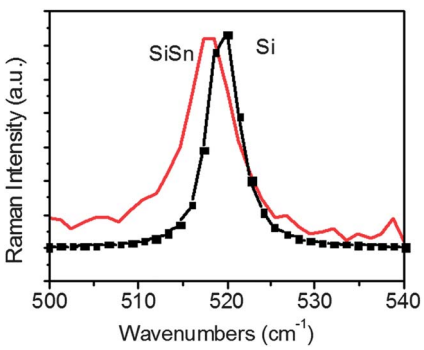

Fig. 2 Raman spectra of the SiSn nanocrystal sample prepared by ns laser ablation in water (red line) and Raman signal of a crystalline Si wafer shown for comparison (black line/squares).

While TEM and EDS analysis would contribute to support the formation of SiSn-NCs, in order to further confirm this hypothesis we have performed selected area electron diffraction (SAED) analysis on the synthesized samples from Fig. 1. The TEM analysis of Fig. 1 revealed a considerable amount of nanocrystals with sizes below the quantum confinement limit of silicon (~10 nm); a high magnification TEM image of the SiSn-NCs is shown in Fig. 3a and the diffraction pattern is shown in Fig. 3b. Fig. 3b illustrates the presence of clear spots arranged in concentric rings which are typical of a polycrystalline material or an ensemble of nanocrystals placed with random orientations.

Specifically, at least four ring patterns can be observed from which the *d*-spacing, as marked by A, B, C, and D, and corresponding values of the unit cells (a) could be evaluated. Two *d*-spacing for each one of the four rings were measured and the mean value calculated. The calculated *d*-spacings are A: 2.47 Å, B: 2.15 Å, C: 1.40 Å, and D: 1.20 Å, which can be indexed to the (211), (220), (331) and (422) planes of a face-centred cubic unit cell with the cell parameter $a = 6.08$ Å. Bearing in mind that both Si and Sn can have a cubic structure with the unit cell dimensions of Si, $a = 5.431$ Å and Sn, $a = 6.473$ Å,[2] the observed unit cell parameter of 6.08 Å, which falls in between them, indicates that the crystallites are indeed an alloy of Si and Sn.

When compared with elemental Si-NCs, SiSn alloyed nanocrystals with quantum confinement effects are expected to present different optoelectronic properties and PL analysis can provide valuable information about their optical behaviour. Fig. 4 shows a typical room temperature PL spectrum of an as-prepared SiSn-NC colloid after ns laser processing (full line/symbols). Unfortunately the PL of the colloid after laser ablation shows very weak PL properties at room temperature (the large PL signal below 500 nm is due to scattering of the 400 nm excitation source on SiSn nanoparticles dispersed in water and filtered through the 400 nm low cut-off optical filter). As we also expect the surface characteristics to play a role in determining the optical properties, we have surface-engineered the SiSn-NCs by microplasma-induced liquid chemistry in water with the intention of reducing potential surface defects and eliminating non-radiative pathways.[21] The open symbols of Fig. 4 show the PL spectrum after surface engineering for 32 min. As can be seen, an increase in the PL intensity located around 620 nm (indicated by an arrow) could be clearly detected.

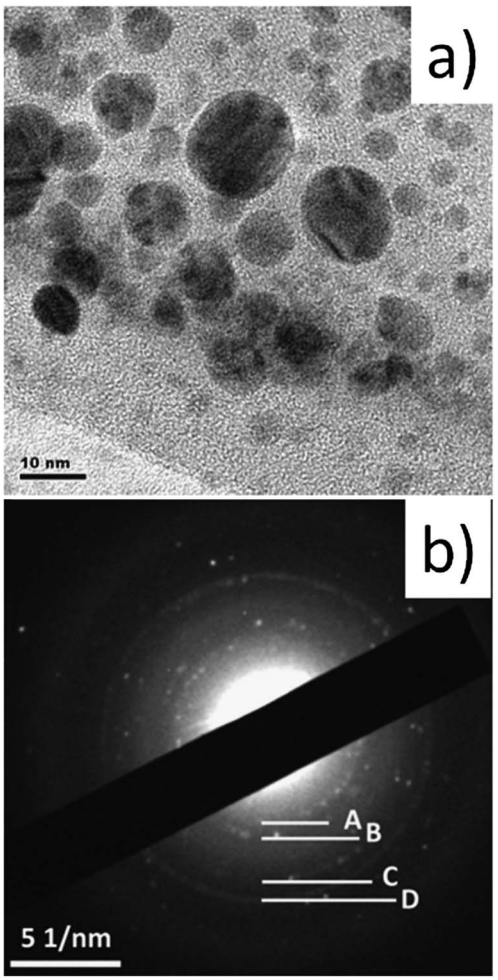

Fig. 3 (a) Transmission electron microscopy (TEM) image of SiSn nanocrystals produced by ns pulsed laser ablation in water of a SiSn target. (b) Corresponding diffraction pattern showing spots arranged in four concentric rings around a central very bright spot, marked by A, B, C, D.

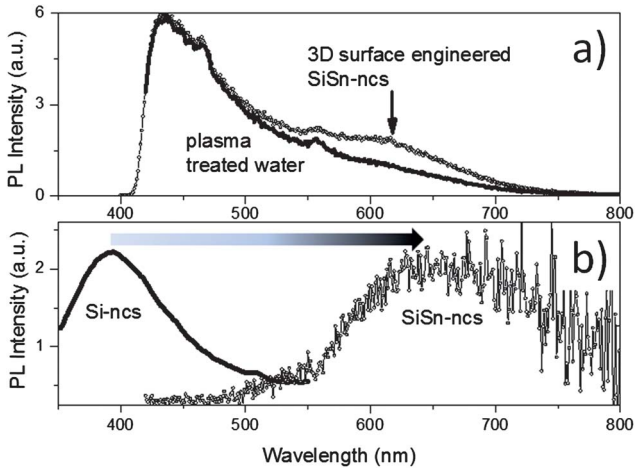

Fig. 4 (a) Photoluminescence (PL) spectra of the SiSn nanocrystal (SiSn-NC)–water colloid as-prepared by ns laser processing (full line) and after microplasma surface engineering for 32 minutes (open symbols/full line); excitation at 400 nm. (b) PL spectrum (400 nm excitation) of the SiSn-NCs after extraction of the background (open symbols/full line) and, for comparison, typical PL spectrum of elemental Si-NCs prepared by ns laser ablation in water and excited with wavelength at 300 nm.

Our results indicate that surface engineering in water induces surface chemistry, which together with quantum confinement, leads to the SiSn-NCs' PL emission properties at room temperature. After background extraction, the PL emission is clearer (Fig. 4b, open symbols/full line) and exhibits a typical broadening due to the large size distribution of the SiSn-NCs. The PL spectrum has a maximum located around 660 nm and it is therefore red-shifted by more than 250 nm compared to the ~400 nm PL peak emission of typical elemental Si-NCs produced under the same conditions (Fig. 4b, full line).[18]

PL analysis suggests the semiconducting character of the SiSn-NCs and the presence of quantum confinement effects. As noted from the PL analysis, the as-prepared SiSn-NCs (and also after 3 months aging in water), the PL at room temperature is very weak.[18] However, PL could be increased after microplasma surface engineering, which indicates the presence of non-radiative surface defects after laser synthesis. The PL maximum is located in the visible range of the spectrum at around 660 nm (1.88 eV); while this wavelength exceeds the energy bandgap of bulk silicon (1.15 eV), it should be noted that quantum confinement is also affecting the PL emission and therefore the PL shift and corresponding bandgap reduction should be considered with respect to elemental Si-NCs. The incorporation of Sn in quantum confined Si-NCs is expected to lower Si-NCs absorption edges and red-shift the PL maximum. Our results in Fig. 4b are consistent with this analysis where a clear PL red-shift from 400 nm to 660 nm is observed (Fig. 4b, indicated by an arrow), which suggests bandgap reduction has taken place due to Si–Sn alloying in the quantum confined nanocrystals.

Our investigations and analysis (Raman, TEM and room temperature PL) suggest that alloying has occurred between Si and Sn, resulting in the synthesis of semiconducting SiSn-NCs with quantum confinement effects. The Raman analysis has only provided partial identification of the SiSn-NCs crystalline structure and we have been unable to compare our results with the literature because SiSn-NCs have not been studied before and theoretical models are not available. However our Raman spectroscopy results assume particular importance because of this, as our measurements represent the first Raman study of nanoscale SiSn systems. More systematic studies will be needed for SiSn-NCs in order to identify the combined effect of size and relative Si/Sn concentration on the Raman signal in addition to possible other environmental factors such as oxide-related strains which have certainly formed in our case due to the water-based synthesis route.

The large difference in size between the Si and Sn atoms results in the thermodynamic instability of $Si_{1-x}Sn_x$ alloys due to lattice mismatch and consequent strain energy. It follows that SiSn is less energetically favorable which is conducive to phase segregation. However, SiSn-NCs, due to strains introduced by the nanoscale dimensions, experience a smaller energy difference between the segregated phase and the alloyed phase making the formation of SiSn alloys at the nanoscale more favorable.[23]

Our results showed that plasmas generated by ns pulsed lasers and confined in water can produce favorable conditions for the synthesis of alloyed of SiSn-NCs. Unique kinetically driven chemical reaction paths lead to the necessary processing environment to obtain such alloyed materials. When the laser irradiates the SiSn target, its energy will be absorbed on the surface leading to surface melting, vaporization, and ionization.[24] Within the short pulse duration (10 ns), a high-temperature, high-intensity, and high-pressure plasma plume of Si and Sn atoms is ignited over the laser spot.[25] Subsequently, the plasma plume expands and results most likely in the formation of Si nuclei, due to the low Sn-concentration. These nuclei continue to grow until nearby silicon clusters and Sn atoms are completely incorporated and consumed, with consequent termination of the growth process.[13] The formation of small (<10 nm diameter) SiSn-NCs can be explained by the nucleation and growth theory that applies to Si-NCs synthesis. A higher concentration of ejected atoms, which can be controlled by the irradiation wavelength and by the pulse duration, results in smaller critical sizes of the forming nuclei[13,26] because more Si or Sn atoms can lead to the formation of stable nuclei and therefore to more nanoparticles with quantum confinement dimensions (Fig. 3). This is particularly seen for nanoparticles prepared by short laser wavelengths, *e.g.* 245 nm.[13,18] The concentration of Sn in the target plays an important role during the formation of the nuclei and determining the tensile strain in the SiSn-NCs. As previously mentioned, at quantum confinement sizes (<10 nm), the energy barrier for alloy formation is smaller than in bulk materials because a large fraction of the Sn and Si atoms are in high energy states due to a range of factors such as a re-organized structure of the core, an increased surface curvature and an overall higher surface energy due to the increasing surface-to-volume ratio. Therefore SiSn alloying may be facilitated at the nanoscale and phase segregation may be avoided also for SiSn-NCs with higher Sn concentrations.

The PL maximum of the SiSn-NCs is located in the visible range of the spectrum and is due to both the relatively low concentration of Sn in the ablation target and the synthesis of very small SiSn-NCs where quantum confinement has significantly opened the energy bandgap with respect to bulk SiSn. These results suggest that in order to decrease even further the band gap of the SiSn-NCs, either larger diameter nanocrystals are required or a higher Sn concentration in the target should be used, where the latter is expected to lead to a higher Sn relative concentration in the SiSn-NCs. Short pulsed laser ablation in liquid media with unique chemistry could in principle allow the achievement of such desired properties. The control of Sn concentration is however critical, as $Si_{1-x}Sn_x$-NCs with $x > 0.3$ leads to direct band gap behaviour[2] while exceeding a certain level of Sn concentration might lead to the formation of undesired metallic nanoparticles. Furthermore, the tensile strain (<5%) can contribute to the band gap downshift and might yield a direct transition, which would be particularly significant for SiSn alloys at quantum confinement sizes. Overall, the bandgap energy of alloyed SiSn could become as narrow as 0.46 eV.[27,28]

Conclusions

In summary we showed that room temperature ns laser ablation of silicon–tin targets in water promote the synthesis of alloyed and semiconducting face-centred cubic silicon–tin nanocrystals (SiSn-NCs) with quantum confinement sizes. Our investigations carried out and reported here clearly provided evidence for the feasibility of SiSn-NCs synthesis from a material standpoint. In particular, the confinement of the laser-produced plasma in water generated by short (10 ns) laser pulses has been demonstrated to be a suitable approach for the formation of metastable phases; this is mainly because laser ablation in liquid relies on high pressure in the liquid medium with highly non-equilibrium chemistry. Furthermore we demonstrated that microplasma surface engineering is highly effective for tuning the surface chemistry of SiSn-NCs by providing a uniform passivation layer without using any complex chemistry and/or lengthy surfactants. The PL emission at room temperature is increased after the SiSn-NCs have been surface engineered in water with more than 250 nm red-shift in the PL maximum compared to elemental Si-NCs. While these results are clear evidence of the synthetic feasibility, future work is required to master the synthesis processes and understand both the SiSn-NCs compositional structure and corresponding optoelectronic properties. The structural and surface characteristics of these SiSn-NCs have however demonstrated their great potential with extraordinary opportunities in photonics, light sources, detection of biological agents, water purification to mention a few, and in particular for PVs.

Experimental details

Target preparation

Since SiSn alloying is inherently challenging, to avoid segregation of Sn we used targets with rather low Sn concentrations (<10%). In order to produce the required optoelectronic properties (bandgap tuning and photosensitivity) of the alloyed SiSn-NCs we expected that ~5% Sn concentration should be used.[29] The targets for amorphous SiSn thin films (thickness = 2 μm) were prepared on glass substrates by a parallel plate configuration very high-frequency plasma-enhanced chemical vapor deposition (VHF-PECVD) system under an operating pressure of 0.5 Torr.[29] The bottom electrode was the powered electrode, whereas the top electrode was a grounded electrode with the substrate. The distance between the electrodes was fixed at 30 mm and a VHF bias of 50 MHz was applied. The input power density was varied from 0.1 W cm^{-2} to 2.4 W cm^{-2}. The substrate temperature was kept at 493 K. Vaporized tetramethyltin ($Sn(CH_3)_4$) and silane gas (SiH_4) were used as Sn and Si sources respectively. A SiH_4–H_2 gas mixture (SiH_4–H_2) was introduced into the chamber *via* the powered electrode.[29] The deposition was performed under high hydrogen dilution condition to avoid carbon contamination originating from plasma-induced dissociation of the $Sn(CH_3)_4$ vapor. A mixture of vaporized $Sn(CH_3)_4$ and H_2 was injected from the sidewall of the deposition chamber at 6 sccm with a $Sn(CH_3)_4$: H_2 ratio of 0.001 g min^{-1}. Our experimental conditions resulted in a controlled Sn content with a Sn incorporation at about 5%.[29]

Laser ablation

Our experimental setup for the synthesis of nanocrystals is based on a pulsed laser ablation technique where the laser-produced plasma is confined in water.[13,18] Similar to our previous work, the SiSn-NCs are prepared using a nanosecond pulsed excimer laser (KrF, 245 nm 20 Hz, 10 ns, ~23.5 mJ cm^{-2}). The target (amorphous SiSn thin film on glass substrate) is adhered at the bottom of a glass container and immersed in 10 mL water. The laser beam is focused onto a 1.5 mm diameter spot on the wafer surface by a lens. The glass container is rotated during the ablation process. The ablation process is continued for 10 min at room temperature and ambient pressure.

Three dimensional surface engineering

In order to achieve the required surface characteristics, surface engineering of the SiSn-NCs by a DC atmospheric-pressure microplasma was applied; the microplasma is generated between Ni tubing (inner diameter 0.7 mm, outer 1 mm) and the surface of the SiSn-NCs aqueous colloid.[21] As a counter electrode, a carbon rod (5 mm diameter) was immersed about 5 mm in the solution at a distance of about 3 cm from the nickel tubing. A positive voltage was applied to the carbon rod to sustain 1.5 mA while the nickel tubing was connected to ground through a 100 kΩ resistor. Pure argon was flown inside the Ni tubing at a rate of 25 sccm. The distance between the nickel tubing and the liquid dispersion surface was adjusted at 1 mm. After synthesis by ns laser processing, the SiSn-NC–water colloid was treated by the DC microplasma for about 32 min.

Material characterizations

Transmission electron microscopy (TEM) analysis (both imaging and diffraction), energy-dispersive X-ray spectroscopy (EDS) and Raman spectroscopy were employed to perform structural analysis of the nanoparticles. In order to limit the luminescence contribution to the Raman spectra an excitation wavelength of 633 nm was used to study the SiSn-NCs after evaporation of the water. For the PL measurements (Shimadzu, RF–5300PC) an excitation wavelength of 400 nm was used, obtained from the monochromated output of a Xe lamp. The elemental Si-NCs used for comparison were excited in colloidal solution at 300 nm. Both PL and Raman measurements were performed at room temperature and ambient atmosphere.

Acknowledgements

This work was partially supported by a NEDO project, international network the Leverhulme Trust Grant, and D.M. acknowledges the support of the JSPS Bridge Fellowship and the University of Ulster Strategic Research Fund. The authors would also like to acknowledge Dr Calum Dickinson who contributed to the TEM analysis.

References

1 K. G. Prasad, M. B. Kurup and A. Bhagawat, *Nucl. Instrum. Methods Phys. Res., Sect. B*, 1986, **15**, 698.
2 J. Tolle, A. V. G. Chizmeshya, Y.-Y. Fang, J. Kouvetakis, V. R. D'Costa, C.-W. Hu, J. Menéndez and I. S. T. Tsong, *Appl. Phys. Lett.*, 2006, **89**, 231924.
3 M. Zacharias, J. Heitmann, R. Scholz, U. Kahler, M. Schmidt and J. Bläsing, *Appl. Phys. Lett.*, 2002, **80**, 661.
4 Y. Kuwano, M. Ohnishi, H. Nishiwaki, S. Tsuda, T. Fukatsu, K. Enomoto, Y. Nakashima and H. Tarui, *Proceedings 16th IEEE PV Specialists Conference*, San Diego, CA, 1982, p. 1338.
5 J. L. Corkill and M. L. Cohen, *Phys. Rev. B: Condens. Matter*, 1993, **47**, 10304.
6 J. Kouvetakis, *et al.*, *J. Mater. Chem.*, 2007, **17**, 1649.
7 X. Chi, R. T. Beeler, G. Grzybowski, A. V. G. Chizmeshya, J. Menendez and J. Kouvetakis, *J. Am. Chem. Soc.*, 2012, **134**(51), 20756.
8 R. T. Beeler, D. J. Smith, J. Menéndez and J. Kouvetakis, *Appl. Phys. Lett.*, 2012, **101**(22), 221111.
9 Y. Kwon, *et al.*, *Chem. Mater.*, 2007, **19**, 982.
10 M. Beard, K. P. Knutsen, P. Yu, J. M. Luther, Q. Song, W. K. Metzger, R. J. Ellingson and A. J. Nozik, *Nano Lett.*, 2007, **7**, 2506.
11 A. J. Nozik, *Chem. Phys. Lett.*, 2008, **457**, 3.
12 I. L. Medintz, H. T. Uyeda, E. R. Goldman and H. Mattoussi, *Nat. Mater.*, 2005, **4**(6), 435.
13 V. Švrček, T. Sasaki, Y. Shimizu and N. Koshizaki, *Appl. Phys. Lett.*, 2006, **89**, 213113.
14 P. Liu, H. Cui, C. X. Wang and G. W. Yang, *Phys. Chem. Chem. Phys.*, 2010, **12**, 3942.
15 D. Rioux, M. Laferrière, A. Douplik, D. Shah, L. Lilge, A. V. Kabashin and M. M. Meunier, *J. Biomed. Opt.*, 2011, **14**, 021010.
16 C. L. Sajti, R. Sattari, B. N. Chichkov and S. Barcikowski, *J. Phys. Chem. C*, 2010, **114**, 2421.
17 R. Intartaglia, K. Bagga, F. Brandi, G. Das, A. Genovese, E. Di Fabrizio and A. Diaspro, *J. Phys. Chem. C*, 2011, **115**, 5102.
18 V. Švrček, D. Mariotti and M. Kondo, *Opt. Express*, 2009, **17**, 520.
19 V. Švrcek, D. Mariotti, T. Nagai, Y. Shibata, I. Turkevych and M. Kondo, *J. Phys. Chem. C*, 2011, **115**, 5084.
20 D. Mariotti, S. Mitra and V. Švrcek, *Nanoscale*, 2013, **5**(4), 1385.
21 V. Švrcek, D. Mariotti and M. Kondo, *Appl. Phys. Lett.*, 2010, **97**, 161502.
22 D. Mariotti, V. Švrcek, W. J. Hamilton, M. Schmidt and M. Kondo, *Adv. Funct. Mat.*, 2012, **22**, 954.
23 R. V. S. Jensen, *J. Phys.: Condens. Matter*, 2011, **23**, 345501.
24 M. S. Tillack, D. W. Blair and S. S. Harilal, *Nanotechnology*, 2004, **15**, 390.
25 F. Mafuné, J. Kohno, Y. Takeda and T. Kondow, *J. Phys. Chem. B*, 2000, **104**, 9111.
26 G. Z. Cao, *Nanostructures and Nanomaterials: Synthesis, Properties and Applications*, Imperial College Press, London, 2004, ch. 3.
27 J. Safarian, L. Kolbeinsen and M. Tangstad, *Metall. Mater. Trans. B*, 2011, **42**, 853.
28 R. V. S. Jensen, T. G. Pedersen and A. N. Larsen, *J. Phys.: Condens. Matter*, 2011, **23**, 345501.
29 T. Nagai, T. Kaneko, Z. Liu, I. Turkevych and M. Kondo, *J. Non-Cryst. Solids*, 2012, **358**, 2281.

